Published in: *Journal of Membrane Science 544 (2017) 278–286*

Structural and chemical stability of high performance $Ce_{0.8}Gd_{0.2}O_{2-\delta}$ - $FeCo_2O_4$ dual phase oxygen transport membranes

M. Ramasamy,[a] E. S. Persoon,[b] S. Baumann,[*,a] M. Schroeder,[b] F. Schulze-Küppers,[a] D. Görtz,[b] R. Bhave,[c] M. Bram[a], W.A. Meulenberg[a]

a) Forschungszentrum Jülich GmbH, Institute of Energy and Climate research, Materials Synthesis and Processing (IEK-1), D-52425 Jülich, Germany, E-Mail: s.baumann@fz-juelich.de
b) Institute of Physical Chemistry, RWTH Aachen University, D-52074 Aachen, Germany
c) Materials Science & Technology Division, Oak Ridge National Laboratory, Oak Ridge, TN 37831, USA

Abstract

Ceramic oxide membranes are widely being researched for Carbon Capture and Storage/Utilization sector applications. Foreseen applications of these membranes are oxygen generation for oxyfuel combustion in e.g. power plants, glass-, cement- or steel production. Major drawback with Mixed Ionic and Electronic Conducting (MIEC) perovskite structure membranes is their limited long term stability at high temperatures in aggressive atmospheres. Dual phase composite membranes have been reported to excel overcoming this drawback. In addition to performance evaluation, $Ce_{0.8}Gd_{0.2}O_{2-\delta}$ - $FeCo_2O_4$ (CGO-FCO) membranes were subjected to stability test in flue gas conditions closely mimicking industrial flue gas atmosphere. The dual phase composites are investigated for their phase stability at the operating temperature of 850 °C in a gradient of oxygen chemical potential. The composites were also exposed to a series of gas mixtures over a period of time at their operating temperature to test for the chemical stability. CGO-FCO membranes are identified to possess chemical stability in gas mixtures of CO_2, SO_2 along with oxygen over a period of 200 h at 850 °C under oxygen partial pressure gradient.

Introduction

Oxygen transport membranes (OTM) gained interest with the identification of the MIEC perovskite compounds ABO_3 [1]. OTMs find potential applications in power plants and industries for oxyfuel combustion. OTMs are also most relevant in catalytic membrane reactors for partial oxidation of methane (POM) to syngas and oxidative coupling of methane (OCM) to higher hydrocarbons such as ethylene and ethane[2]. In fossil fuel power plants and industries such as cement, steel and glass production, the oxygen separation process includes exposure to flue gases containing CO_2, SO_x, dust, and steam. Thus, stability in flue gases at high temperature and oxygen partial pressure gradient is critical for an oxygen transport membrane[3, 4]. State of the art OTMs such as LSCF and BSCF, in spite of their exceptional permeability for oxygen, proved to be unstable in harsh flue gas conditions. Phase instability and carbonate/sulphate formation at elevated temperatures have been reported for these MIEC OTMs[1, 5, 6]. Dual phase membranes on the other hand are composite materials expected to provide efficient oxygen permeation and high chemical stability under exhaust gas conditions[3, 7-10]. Research on stability of both MIEC perovskites and dual phase composites are mostly concerning the impact of CO_2 on OTMs [11-14], but very little on impact of SO_2 and H_2O gases though these gases also constitute to re-circulated flue gas stream in power plants[15]. Hence stability testing of membranes in CO_2 and SO_2 containing gas mixture would be essential for their industrial applicability.

In this paper, a Fluorite-Spinel composite $Ce_{0.8}Gd_{0.2}O_{2-x}$ - $FeCo_2O_4$ (CGO-FCO) reported to have good oxygen permeability will be investigated. In this dual phase composite, CGO, a pure ionic conducting phase is combined with FCO, a pure electronic conducting phase to provide the necessary mixed ionic electronic conduction for efficient oxygen transport. In our previous work, we discussed in detail about the phase interaction and secondary phase formation in the 60 wt% CGO with 40 wt% of FCO (54 vol% CGO – 46 vol% FCO) composites represented as 60CGO-FCO. A secondary phase $GdFeO_3$ orthorhombic perovskite with substitution of Ce and Co (GCFCO) is formed by the interdiffusion during sintering at 1200 °C[16]. This phase is categorized as a predominant electronic conductor, and should therefore contribute to the electron transport in the CGO-FCO membrane. We also reported that the highest oxygen flux was achieved for 85CGO-FCO composite with the volume fraction of the minor phase, only 18.5 vol%[17], contrary to the hypothesis that the percolation threshold can be reached only if the volume fraction of the minor phase is no less than 30 vol% for a dual-phase material[18]. In this paper, the 60CGO-FCO and 85CGO-FCO composites have been categorically compared in depth based on their microstructure, performance and stability to identify the most prominent OTM composite composition.

Experimental

The $Ce_{0.8}Gd_{0.2}O_{2-\delta}$ – $FeCo_2O_4$ composite powders (XCGO-FCO with X = wt% of CGO) were synthesized by the modified one pot Pecchini synthesis[19]. Phases were identified and their distribution was analysed using a XRD - diffractometer D4 ENDEAVOR (Bruker AVS) with CuKα radiation, $\Delta 2\theta = 0.02°$ and a SEM - Zeiss Ultra 55 (EDS INCAEnergy355 INCA Crystal) and a Zeiss Supra 50 VP (Carl Zeiss NTS GmbH) respectively. X-ray analysis data was further subjected to Rietveld refinement for semi-quantification of the phases present after the sintering process in air. Disc shaped Membranes were sintered at 1200 °C for 10 h for stability testing and permeation measurements. The composites were also measured for electrical conductivity using a 4 point DC probe method on bar shaped dense samples.

Permeation experiments were performed with 1 mm thick and 15 mm diameter membranes after polishing the surfaces on both sides with SiC paper and 3 µm diamond paste. The membranes were then sealed with two gold rings in an asymmetric glass tube setup[20]. The membrane was heated to 1000 °C while pressure was applied to the gold ring sealing. Initial short term permeation measurements were carried out between 650 and 1000 °C, with air and argon as feed and sweep gas at a flow rate of 250 and 50 ml/min, respectively. To avoid any limitations of the oxygen flux due to sluggish surface oxygen exchange, screen printing of a porous ~ 10 µm thick activation layers of LSCF ($La_{0.58}Sr_{0.4}Co_{0.2}Fe_{0.8}O_{3-\delta}$) on the membranes post-sintered at 1050 °C for 5 h[16]. In addition, 60CGO-FCO and 85CGO-FCO samples without catalytic layer were short term permeation tested.

Chemical stability of the samples was tested by annealing experiments in various gas mixtures. Samples of the composites 60CGO-FCO and 85CGO-FCO were sintered and ground to the size 10mm diameter to ensure optimal fitting into the apparatus. Four sets of the samples were prepared for stability testing in varying combinations of gas mixtures to closely mimic the possible flue gas mixture in industrial conditions as listed here; 1) Pure CO_2 2) 250 ppm (volume parts per million) of SO_2 in CO_2 3) 250 ppm SO_2 + 5 vol% O_2 in CO_2 4) 250 ppm SO_2 + 5 vol% O_2 + 2.5 vol% H_2O (saturated at room temperature) in CO_2. The samples were annealed in a tube furnace at 850 °C for 16 h allowing the above mentioned gas mixtures to flow over the sample for the dwell time of the experiment. In addition, a long

term annealing of a 60CGO-FCO sample was carried out at 850 °C for 1000 h in an atmosphere of 100 ppm SO_2 / 5% O_2 / Ar. Post characterization of the tested samples involved surface analysis by XRD using EMPYREAN, PANalytical instruments and SEM-EDS using HITACHI S-4800. The long term stability tests of 60CGO-FCO and 85CGO-FCO were also conducted in oxygen partial pressure gradient without LSCF catalytic layer by annealing the samples at 850 °C for duration of 300 h, including 200 h of exposure to SO_2 at the low p_{O2} side. Air was applied to one side of the membrane with a flow rate of 350 ml/min. On the other side, pure argon gas was flowed for initial 72 h, followed by an argon and SO_2 mixture for 200 h, and again pure argon for the remaining 28 h. A flow rate of 50 ml/min on the low p_{O2} side was maintained at all times during the annealing experiment in spite of 100 or 500 ppm of SO_2 concentration being admixed to the argon during the 200 h interval span. In addition, a similar experiment was conducted with 85CGO-FCO in order to investigate the influence of SO_2 on the oxygen permeation. On the feed side again 350 mL/min syn. air was used. In contrast to the stability tests in a p_{O2}-gradient, Helium was used as sweep gas instead of Argon. The oxygen concentration was measured with a GC Agilent 7890A and a 5Å Molsieve column. The experiment was again divided into three parts, with He sweep gas in the first and last section each lasting for 48 h and 500 ppm SO_2 / He sweep gas in the middle section lasting for 200 h. XRD analyses were performed on pellet surfaces with a STOE Theta–Theta reflection diffractometer with Cu K_{α} radiation. A SEM by LEO/Zeiss (1450VP, Jena, Germany) with an Oxford INCA EDS system was applied.

Microstructure Analysis

The as-prepared 60CGO-FCO and 85CGO-FCO composites are compared for the phases present using their X-ray diffractograms as shown in Figure 1

The decrease in spinel content can be observed from the decrease in intensity of the spinel peaks for the 85CGO-FCO composite in comparison to 60CGO-FCO composite particularly at 2θ = 38°. In addition, the presence of orthorhombic perovskite peaks of GCFCO [17] (between 24° and 33° 2θ) is confirmed in both compositions. Rietveld refinement of the diffractograms was used to obtain semi-quantification of the phases present in the both composites (Table 1). The values also indicate that irrespective of the spinel content, perovskite phase is formed to the same extent as the spinel vanishes. Another important observation is the presence of two spinel phases with a slight difference in their lattice parameter. This lattice parameter difference could be corresponded to the difference in Co/Fe concentration in their estimated stoichiometric spinel composition following Vegard's behaviour [19]. These results are further supported by the SEM images as shown in Figure 2.

Published in: *Journal of Membrane Science 544 (2017) 278–286*

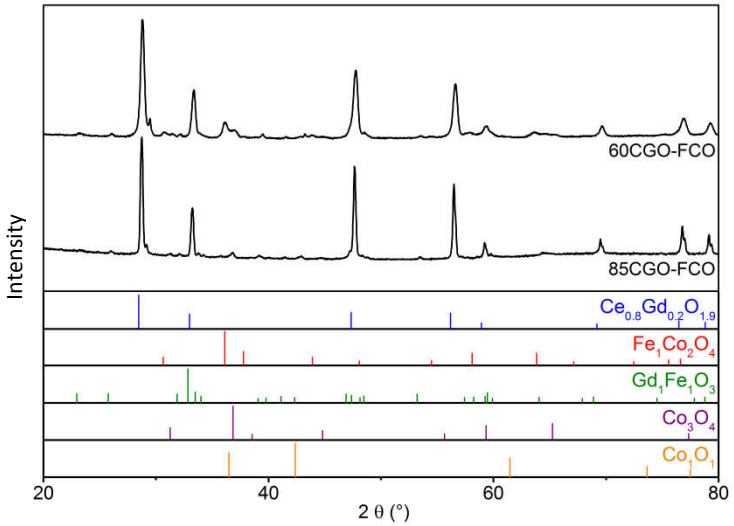

Figure 1 XRD plots of the 60CGO-FCO and 85CGO-FCO composites sintered at 1200 °C for 10 h in air and reference patterns for individual phases.

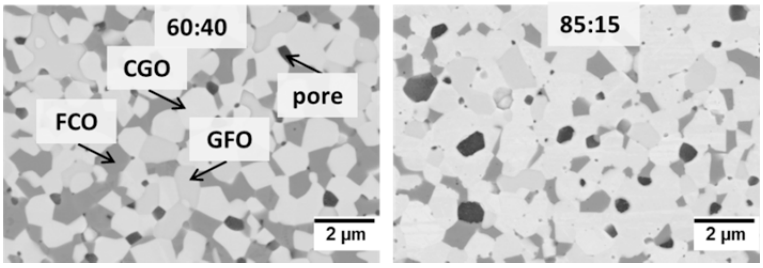

Figure 2 SEM images of 60CGO-FCO (left) and 85CGO-FCO (right) composites sintered at 1200 °C for 10 h in air.

Table 1 Quantification of the phases formed in CGO-FCO composite after sintering at 1200 °C for 10 h in air using Rietveld analysis.

Crystal system-structure	60CGO-FCO		85CGO-FCO	
	Fraction (wt %)	Lattice parameter a (Å)	Fraction (wt %)	Lattice parameter a (Å)
CGO (Cubic – Fluorite)	58	5.417	83	5.418
FCO (Cubic – Spinel)	14	8.309	4	8.300
	18	8.147	5	8.159
(Co, Fe)O (Cubic - Rock salt)	3	4.260	-	-
GdFe (Ce,Co) O_3 Orthorhombic -Perovskite	7	a = 5.337 b = 5.612 c = 7.653	8	a = 5.336 b = 5.613 c = 7.656

The images show the presence of fluorite phase (“lightest” grey) with decreasing fraction of the spinel phase (dark grey) corresponding to the ratio and the presence of orthorhombic perovskite phase (light grey) in both the cases [20]. Moreover, one can see some remaining closed pores (black). Semi quantitative determination of the elements from a STEM/EDS elemental mapping [17] provides an approximate composition of the perovskite phase that is formed in these dual phase composites during the sintering process. As Ceria is expected to

replace Gd on A-sites and Co to replace Fe on B-sites of $GdFeO_3$ perovskite phase, the composition is estimated to be $Gd_{0.85}Ce_{0.15}Fe_{0.75}Co_{0.25}O_3$ (GCFCO). This GCFCO phase is formed as individual grains with no obvious grain boundary phase visible at this magnification.

Electrical Conductivity

Bar shaped samples of the composite and their corresponding single phase materials were fabricated and subjected to electrical conductivity measurements by the four point DC method. The electrical conductivity results of 85CGO-FCO ratio are compared to standard composition 60CGO-FCO, pure CGO, FCO, and GCFCO. Figure 3 shows the compiled results of the dual phase composites and the single phase materials constituting the composite for direct comparison.

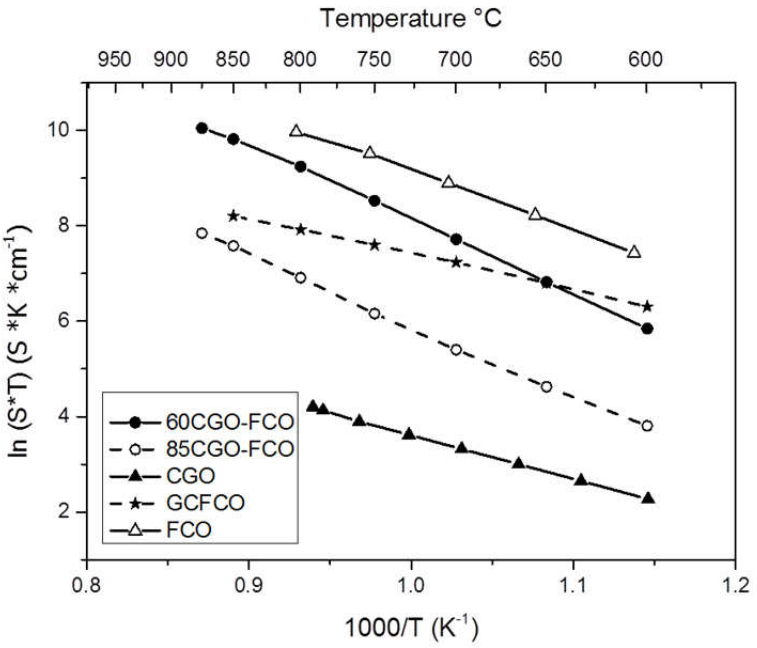

Figure 3 Total electrical conductivities of CGO-FCO composites and their corresponding individual phases measured by four point DC method in ambient air (lines are a guide to the eye).

The electrical conductivity of FCO (purely electronic) is the highest as expected followed by composite with higher spinel content indicating that the electronic conductivity is still dominant. The conductivity decreased with the spinel content reduced to 15 wt%. Nevertheless, the 85CGO-FCO sample still shows higher total conductivity than CGO (purely ionic). This signifies the presence of a percolating network of electronic conductor even with as low as 15 wt% (18.5 vol%) of nominative spinel content. GCFCO as an individual phase has high electrical conductivity and negligible ionic conductivity concluded from a permeation measurement of pure GCFCO bulk membrane resulting in zero permeation (not shown here) [14, 20]. Thus, it is believed that GCFCO, along with the spinel establishes a percolative network potentially at the grain boundaries for electronic conduction in the composite, although the Rietveld analysis revealed a total of only 17 wt% of electronic conductive phases (spinel and perovskite) after sintering, Table 1.

Permeation measurements

CGO-FCO composites with varying composition were tested with regard to their oxygen permeation rate using porous LSCF catalytic coatings on both sides of the disc shaped membranes reducing limitation of surface exchange kinetics. Starting from 60 wt% the percentage of CGO was increased in order to maximize the volume of the ionic conducting phase. In consequence, the permeation rate increases up to a maximum at 85 wt% of CGO. Above that point the permeation rate decreases again probably due to insufficient electronic conductivity in the composite as shown in Figure 4. A significant permeation rate can be measured although the nominative proportion of the electronically conductive spinel phase (15 wt% ≈ 18.5 vol%) is well below the percolation threshold [17], which is in agreement with the electrical conductivity measurements. This effect is already reported a few times without knowing the exact reason [10],[21],[22].

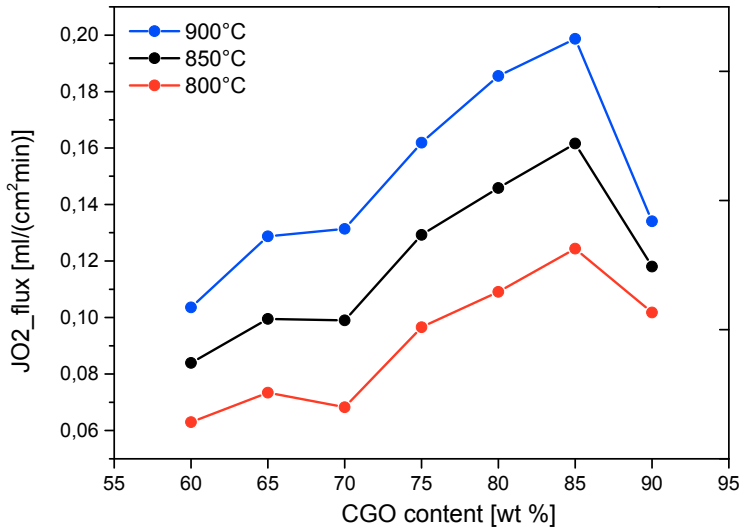

Figure 4 Permeation rate for the surface activated CGO-FCO composites with varying composition under an air/argon oxygen partial pressure gradient (lines are a guide to the eye).

The 60CGO-FCO and 85CGO-FCO composites with and without catalytic layers on both sides of the membranes, were subjected to permeation measurements. Catalytic porous layer coating of LSCF over the composite addresses the surface exchange limitation observed in samples without activation. The permeance of the samples is calculated by Eq. (1), normalizing the partial pressure gradient that are plotted against the operating temperature range in Figure 5.

$$permeance = \frac{j_{O_2}}{\ln \frac{p'_{O_2}}{p''_{O_2}}} = \frac{1}{L} \cdot \frac{R}{16 \cdot F^2} \cdot \sigma_i T \qquad (1)$$

The activation energy E_a is calculated from the permeance as shown in Table 2. The samples without LSCF catalytic layer show high activation energy at lower temperatures (650 – 800 °C) indicating the impact of surface exchange limitations that are overcome by the catalytic layer witnessed in Figure 5. At higher temperatures (800 – 1000 °C), in case of 40 wt% spinel containing composite, the E_a is approx. 66 kJ/mol indicating that the ionic conduction of CGO is the rate limiting step[23]. In the 15 wt% spinel containing composite, the activation energy decreases (55 kJ/mol) indicating a change in the limiting transport process[17].

Summarizing the permeance and activation energy results, 85:15 ratio proves to be a good composition mixture with the highest oxygen flux measured. It can be stated that in an

85CGO-FCO bulk membrane, 85 wt% CGO contributing to the ionic transport, while GCFCO and FCO phases are responsible for electronic transport. Hence efficient percolating networks are formed for both electronic and ionic transport providing a high oxygen flux.

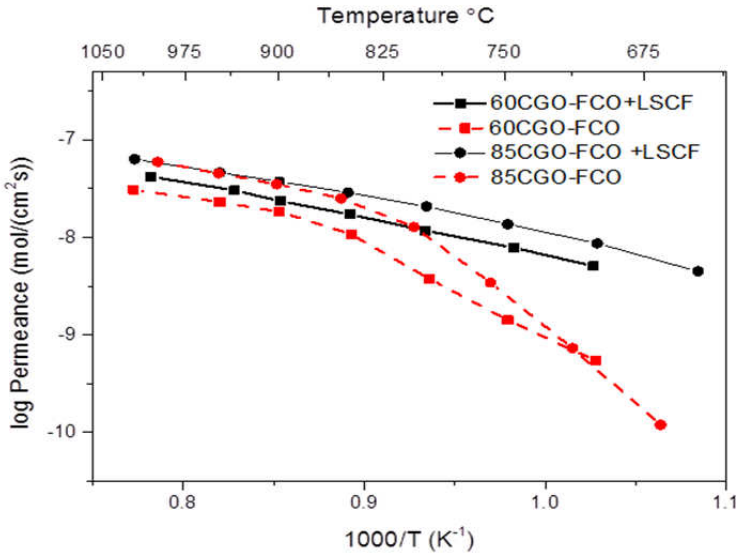

Figure 5 Arrhenius- plot of permeance for the CGO-FCO composites under an air/argon oxygen partial pressure gradient (lines are a guide to the eye).

Table 2 Activation energy of the dual phase composites with and without catalytic layer for a temperature range of 650 -1000 °C.

Sample ID	High temperature (1000 – 850 °C) E_a (kJ/mol)	Low temperature (800 – 650 °C) E_a (kJ/mol)
60CGO-FCO	70	140
60CGO-FCO +LSCF	66	92
85CGO-FCO	70	285
85CGO-FCO +LSCF	55	79

Chemical stability

Dual phase membranes require long term stability in presence of aggressive atmospheres such as CO_2, SO_2, and H_2O. However, in order to identify the impact of each gas element on the stability of the membrane, initially short term stability experiments were carried out at the operating temperature of 850 °C (temperature chosen based on power plant operating conditions). SO_2, O_2, and H_2O gases were mixed in pure CO_2 in a sequence and each combination was tested for the same time interval and temperature in a steel housing. The post characterization of the tested samples is carried out.

The SEM images (Figure 6) show the surface of the 60CGO-FCO sample after exposure to different gas mixtures. In case of pure CO_2 and 250 ppm of SO_2 in CO_2, the samples do not show any variation indicating the stability of the composite in the pure SO_2, CO_2 gas mixture. Upon adding of 5 vol% O_2, the spinel phase (dark grey) grains seem to have surfaced in comparison to the fluorite phase (bright/white) grains. In addition, sulphur containing flakes were identified by EDS and XRD of the sample. Lastly, ~ 2.5 vol% H_2O was added to the gas mixture by passing through a water bubbler (saturated steam at room temperature) (Figure 6D).

EDS mapping of the composite is shown in Figure 7. It can be noticed that Co rich spinel and fluorite grains are visible and are mapped along with sulphur mapping. The backscattered image portrays distribution of sulphur containing flakes on top of both spinel and fluorite grains at the surface level.

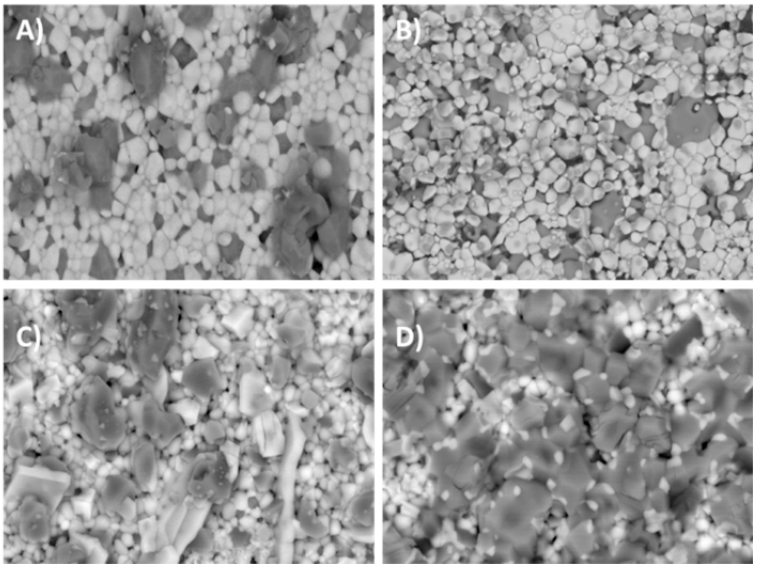

Figure 6 SEM images of 60CGO-FCO composite after exposure at 850 °C for 16 h to A) Pure CO_2 B) 250 ppm of SO_2 in CO_2 C) 250 ppm SO_2 + 5 vol% O_2 in CO_2 and D) 250 ppm SO_2 + 5 vol% O_2 + 2.5 vol% H_2O (saturated at room temperature) in CO_2.

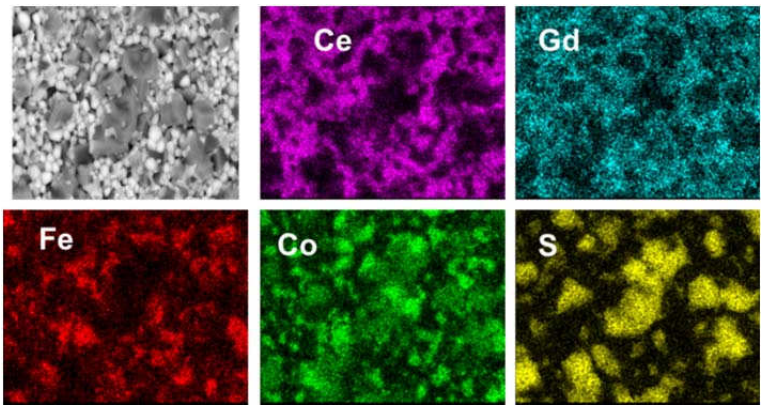

Figure 7 EDS analysis of 60CGO-FCO composite after exposure 250 ppm of SO_2 in CO_2 + 5 vol% O_2 + 2.5 vol% H_2O at 850 °C for 16 h.

However, the cross-sectioned sample (not shown here) does not show the presence of sulphur except for the surface revealing no chemical sulphur interaction with the individual phases of the composite.

The experiments were repeated for 85CGO-FCO samples to determine its behaviour under similar conditions. Figure 8 shows the SEM surface images of the 85CGO-FCO samples after exposure to the four gaseous mixtures during the annealing process for 16 h. The SEM images of 85CGO-FCO indicate similar behaviour as 60CGO-FCO samples in these test conditions. Addition of 5 vol% O_2 marks the beginning of sulphur containing flakes observed on the surface and the condition intensifies with 2.5 vol% H_2O inclusion. However there were no traces of sulphur reaction with the phases of the composite forming sulphates. It is important to consider that these flakes probably be attributed to interaction of SO_2 with dust or galled steel impurities in the presence of O_2 and H_2O. Thus it can be stated that both these dual phase composites are stable towards the tested atmospheres.

However, these flakes accumulation will probably also form in real devices and over a long run might contribute to adverse effect on the effectiveness of the oxygen transport when settling down on the membrane surface. Hence, long term tests in real flue gas (containing fly ash) should shed light on this aspect as it has not been reported or investigated so far.

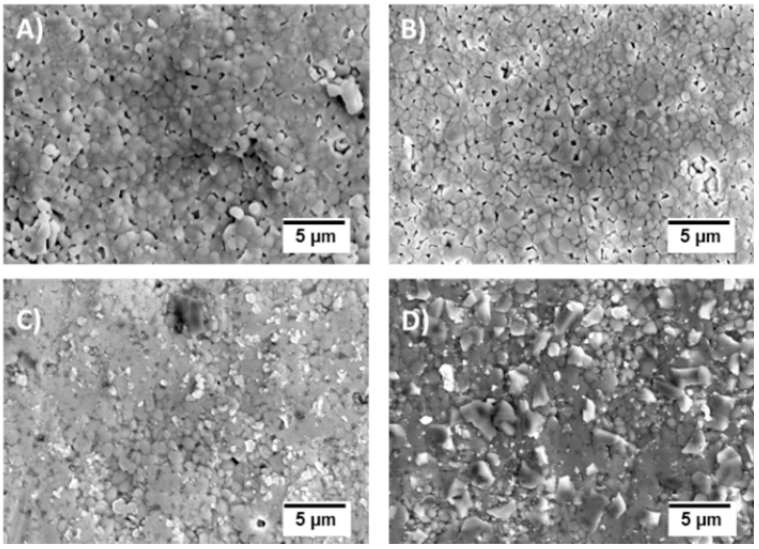

Figure 8 SEM image of 85CGO-FCO composite after exposure at 850 °C for 16 h A) Pure CO_2 B) 250 ppm of SO_2 in CO_2 C) 250 ppm SO_2 + 5 vol% O_2 in CO_2 and D) 250 ppm SO_2 + 5 vol% O_2 + 2.5 vol% H_2O (saturated at room temperature) in CO_2.

As a long term stability test, 60CGO-FCO composite was annealed for 1000 h at 850 °C in an atmosphere of 100 ppm SO_2 / 5% O_2 / Ar in a ceramic housing. These SO_2 and O_2 concentrations are comparable to concentrations in Oxyfuel cement plants. Comparing the diffraction pattern of the sample surface (Figure 9) before and after the exposure it can be observed that no new phases have been formed during the stability test. The broad $FeCo_2O_4$ spinel reflex has been shifted to smaller angels and has narrowed.

The SEM/EDS analysis indicates that the sample surface (Figure 10) has roughened compared to the polished surface of the as prepared sample. The presence of minor sulphur concentrations at the surface cannot completely be ruled out from the EDS Spectra (Figure 10) as there might be a spectral interference between the sulphur Kα-peak at 2.31 keV and the gold Mα-peak at 2.12 keV. However, taking into account the absence of any sulphur related reflexes in the X-Ray diffractograms, we conclude that a chemical reaction with SO_2 has not taken place and results show that 60CGO-FCO is stable in 100 ppm SO2 for 1000 h at 850 °C. No degradation of any phase could be detected.

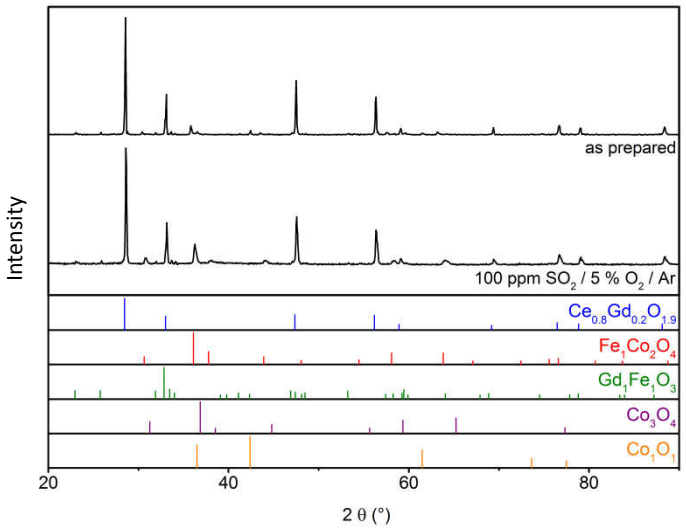

Figure 9 XRD intensity plots of 60CGO-FCO as prepared and after 1000 h exposure to 100 ppm SO_2/ 5% O_2 / Ar at 850 °C.

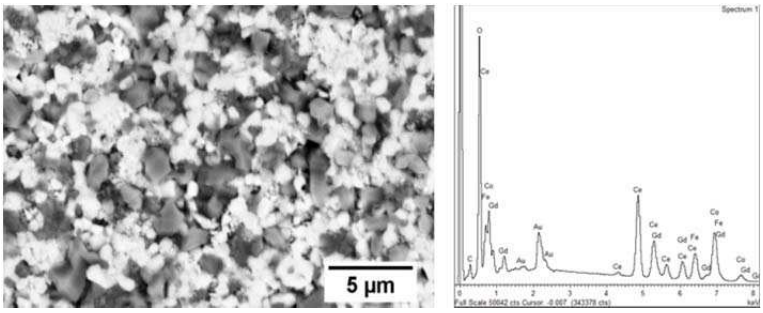

Figure 10 SEM image and SEM-EDS Spectrum of 60CGO-FCO after annealing in 100 ppm SO_2 / 5 vol% O_2 / Ar at 850 °C for 1000 h.

Structural stability and phase segregation in p_{O2}-gradient

60CGO-FCO

The 60CGO-FCO sample after permeation measurements was noticed to have different colour on one side of the surface. Thus SEM surface analysis after permeation measurement was carried out. Figure 11 shows the SEM cross section at the high p_{O2} surface of the 60CGO-FCO sample. Analysis revealed that there are large dark crystals on the surface at the high p_{O2} side of the composite. On the other hand, the low p_{O2} side surface of the membrane showed clustered white grains widely distributed. The dark crystals contain predominantly cobalt and iron oxide while the white grains contain cerium and gadolinium oxide. This behaviour is attributed to the segregation of two phases with enrichment of the faster cations at the high p_{O2} side.

In general, the cation deficiency of spinel phase accelerates faster diffusion of Fe and Co cations in comparison to Ce and Gd cations of the fluorite phase [24-26]. According to the Gibbs-Duhem relation the gradient of oxygen chemical potential applied in the permeation test is balanced by a chemical potential gradient of the cations in opposite direction. This chemical potential gradient is the driving force for cation diffusion [27]. The phase segregation might significantly impact long term oxygen permeation of the membrane by surface exchange limitation due to reduced triple phase boundaries or spinel crystals eventually form-

ing a blocking layer, if this is continued. Thus, long term stability test under p_{O2} gradient were carried out to evaluate this hypothesis.

The long term stability tests under p_{O2} gradient were performed on 60CGO-FCO, by exposing the membrane to Ar/ SO_2 sweep gas with varying SO_2 and O_2 concentrations on the low p_{O2} side for 200 h to determine both the chemical stability in SO_2 and the impact of SO_2 on the previously observed phase segregation. The sweep gas contained 100 ppm and 500 ppm SO_2 in Ar. In addition, in a third experiment 5 vol% oxygen was added to the sweep gas in total containing 100 ppm SO_2/ 5 vol% O_2/Ar. As a result, the impact of the oxygen partial pressure gradient on the segregation could be examined. The post-test analysis was conducted with reflective XRD as well as SEM analysis. The XRD diffraction analysis on the as prepared membrane, as well as the high and low p_{O2} sides of both membranes exposed to 100 and 500 ppm SO_2 are shown in Figure 12. The diffraction pattern of the as prepared sample contains the phases CGO, FCO, GFO and small amounts of a rock salt phase, i.e. (Co,Fe)O. The FCO reflex at 36 °2θ is split up into a broad reflex with two maxima. This is due to the presence of the two spinel phases as described in the microstructure section.

The diffraction patterns of the high p_{O2} sides contain peaks that are attributed to Co_3O_4, which is attributed to an enrichment of the spinel in Co the faster cation in FCO. The amount of Co_3O_4 formed at the membrane surface seems to correlate with the SO_2 concentration in the low p_{O2} side gas mixture. An admixture of 5 vol% O_2 reduces the Co_3O_4 phase formation due to the reduced chemical potential gradient leading to slower cation diffusion. Furthermore, the rock salt phase peaks have disappeared on the high p_{O2} side in all the cases as expected from the spinel phase diagram. In contrast, on the low p_{O2} sides no new phases have been formed while the FCO reflex has been narrowed in comparison to the two broad spinel peaks of the as prepared sample. On the low p_{O2} side of the 60CGO-FCO membrane, slight formation of Co_3O_4 spinel phase can be observed that is probably due to the 5 vol% O_2 exposure oxidizing the transition metal oxides. It is noted, that exposure to SO_2 did not lead to formation of any sulphates.

The XRD findings are further underlined by SEM investigations of the membranes. On the high p_{O2} side, large dark crystals (Spinel) grew out of the surface (Figure 13), that measures up to 5 µm in thickness, whereas on the low p_{O2} side a significant amount of pores is visible. The 200 h long SO_2-exposure did not lead to the formation of sulphur containing compounds. This indicates that the membrane material is chemically stable against concentrations up to at least 500 ppm SO_2 for 200 h at 850 °C.

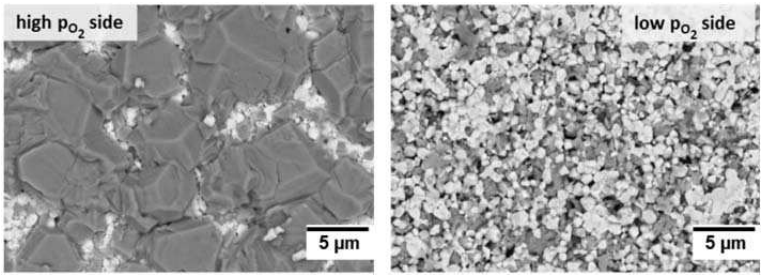

Figure 11 SEM images of 60CGO-FCO membrane after permeation measurement under an air/argon oxygen partial pressure gradient.

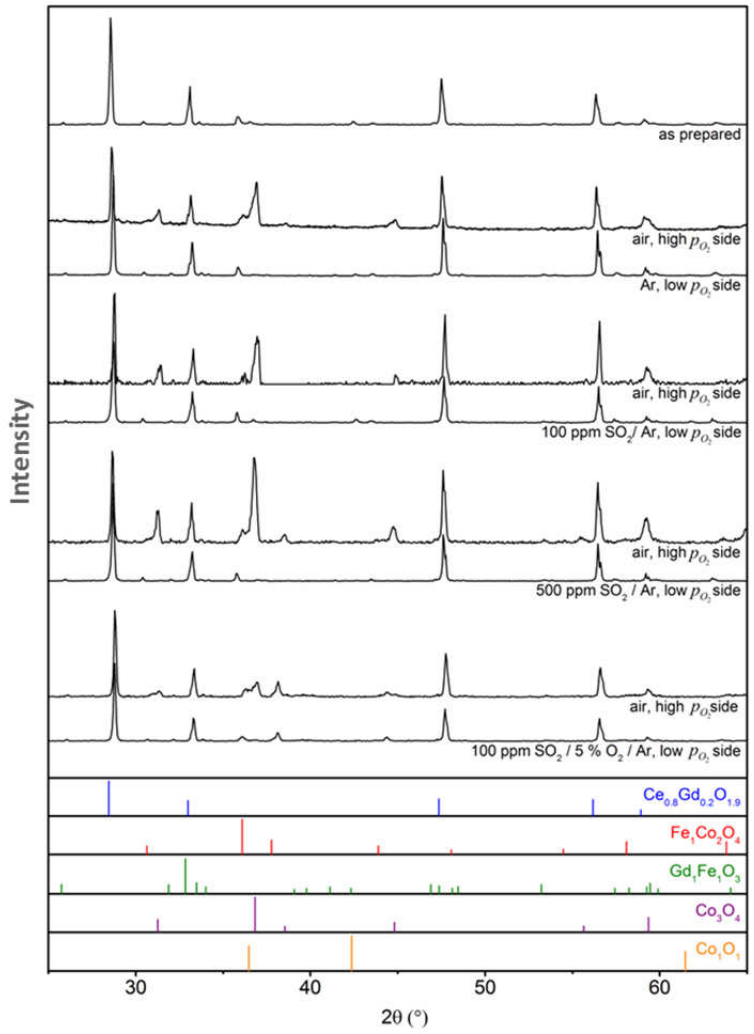

Figure 12 XRD of feed and sweep sides of 60CGO-FCO samples tested in different oxygen partial pressure gradients at 850 °C for 200 h.

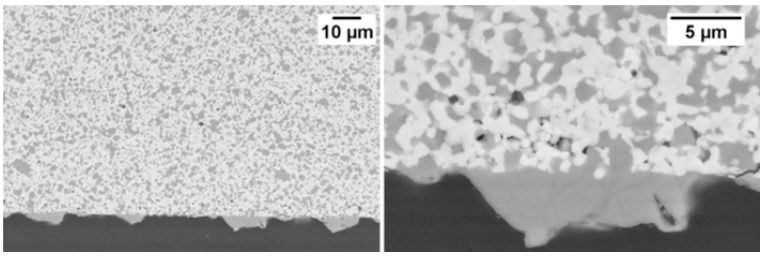

Figure 13 Back scattered electron microscopy (BSEM) image of cross section on the high p_{O2} side of the 60CGO-FCO membrane.

85CGO-FCO

85CGO-FCO composite showed a lesser extent of phase segregation at the high p_{O2} side of the membrane as shown in Figure 14 in comparison to Figure 11. This can be attributed to the lesser spinel-content in this composition. This added advantage further supports the improved phase stability of the lower spinel content CGO-FCO membrane. Similar long term stability tests in a p_{O2} gradient were carried out for 85CGO-FCO membranes exposing them to 100 ppm and 500 ppm SO_2 in Argon on the low p_{O2} side for 200 h. In order to investigate harsher conditions, 500 ppm SO_2 was used in this test.

XRD analysis was likewise performed on the 85CGO-FCO membranes on both the high and low p_{O2} sides shown in Figure 15. Although the segregation effect is much lower, the onset of Co_3O_4 phase formation on the high p_{O2} side can still be observed. However, on the low p_{O2} side, peaks of the FCO spinel phase, which were already low due to the low spinel content, have disappeared.

Summarizing the results on the phase segregation during long term stability test in p_{O2} gradients of 60CGO-FCO and 85CGO-FCO membranes, while exposing the low p_{O2} side to 100 and 500 ppm SO_2, it can be stated that the phase segregation is more severe in the higher spinel containing composite. In addition to the lower volume fraction of the spinel, the formation of GCFCO during sintering might further slowdown the cation diffusion leading to less enrichment of spinel at the high p_{O2} side. There seems also a slight increase of phase segregation in the 500 ppm SO_2 samples compared to the 100 ppm SO_2 samples for the 85CGO-FCO composition sample, which cannot be explained so far. On the high p_{O2} side a formation of a Co_3O_4 phase could be observed that is probably doped with Fe. On the low p_{O2} side an enrichment of the CGO phase took place due to a depletion of the FCO-Phase. Again, there might be a spectral interference between the sulphur Kα-peak at 2.31 keV and the gold Mα-peak at 2.12 keV in the EDS Spectra (Figure 16). However, we conclude, together with the XRD analyses, that a chemical reaction with SO_2 has not taken place.

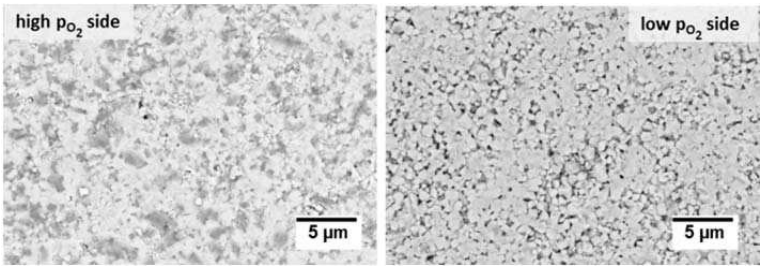

Figure 14 SEM images of 85CGO-FCO membrane after permeation measurement under an air/argon oxygen partial pressure gradient.

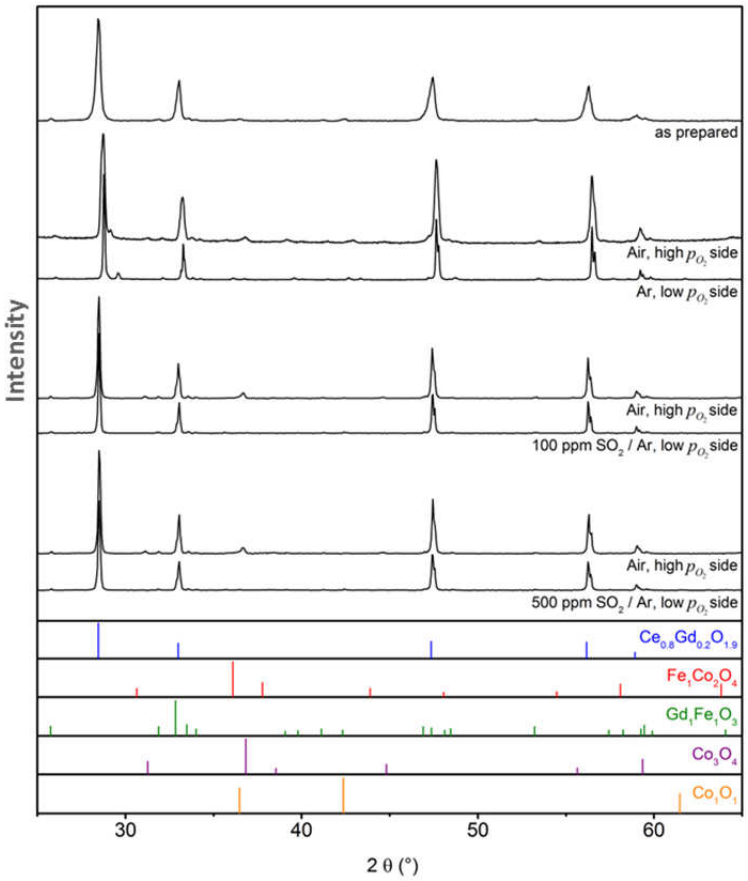

Figure 15 XRD of high and low p_{O2} sides of 85CGO-FCO samples tested in oxygen partial pressure gradient at 850 °C for 200 h.

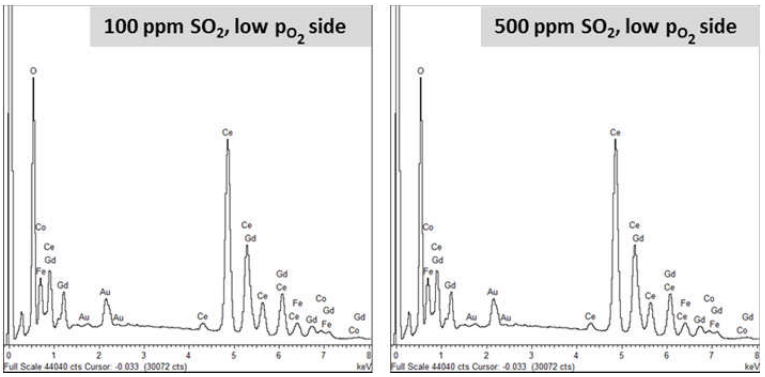

Figure 16 SEM-EDS of 60CGO-FCO samples low pO_2 sides after long term stability test under oxygen partial pressure gradient with varying SO_2 concentrations for 200 h at 850 °C.

Oxygen flux measurement of 85CGO-FCO in contact with SO_2

The oxygen flux $j(O_2)$ was additionally investigated for the 85CGO-FCO composition . The sample was not surface activated in order to investigate purely the membrane material stability without catalyst poisoning effects. The 85CGO-FCO membrane was placed in a p_{O2}-gradient with syn. air on the feed side and He or He with 500 ppm SO_2 on the sweep side. In the first 48 h while only He was used as sweep gas (Figure 17, section I) the oxygen flux increased slightly from 0.050 to 0.054 ml·min^{-1}·cm^{-2} (15 % per 100 h). After adding 500 ppm

SO_2 (section II) the oxygen flux instantaneously dropped by 61 % from 0.054 to 0.021 ml·min^{-1}·cm^{-2} During the SO_2 exposure over the course of 200 h the flux continued to slightly increase to 0.024 ml·min^{-1}·cm^{-2} (9 % per 100 h). After the SO_2 exposure the sweep gas was switched back to pure He (section III) resulting in a slow flux recovery over the course of 24 h to 0.071 ml·min^{-1}·cm^{-2}, which is an even higher value than was measured in section I. Slow flux recovery may be due to either sluggish SO_2 desorption kinetics or because of residual SO_2 that resides in the permeator gas compartment due to poor flushing after gas switching. To verify that the latter effect can be ruled out, we carried out gas switching tests with a non-adsorbing gas (Ar). The tests showed that Ar was flushed out almost instantly, so that it is concluded that the slow flux recovery is determined by SO_2 desorption kinetics.

It has to be noted that the membrane was not surface activated, which has two effects. First, the measured fluxes are very low compared to Fig. 4, so that small changes become relatively significant. Second, the flux is limited by oxygen surface exchange. The instantaneous drop in permeation when SO_2 is introduced into the sweep gas and the complete recovery after switching off is due to competitive surface adsorption of SO_2 partially blocking the active sites for oxygen surface exchange. This effect is already reported for CO_2 sweep e.g. for LSCF membranes [5]. SO_2 obviously has a much larger effect even in low concentrations because of a higher tendency to adsorb as compared to CO_2. Moreover, the surface exchange limitation of the membrane in this experiment increases the importance of the competitive adsorption.

The slight increase of the oxygen flux that occurred during the entire experiment can be explained by the phase segregation and the consequential increase of the surface area by surface roughening. Apparently, this effect slightly facilitates the surface exchange by an increase in triple phase boundaries compared to the polished surface. In conclusion, CGO-FCO sustains a significant and stable oxygen flux even in SO_2 containing atmospheres, but a higher demand of membrane area has to be considered in application depending on temperature, amount of impurities, and degree of surface exchange limitations.

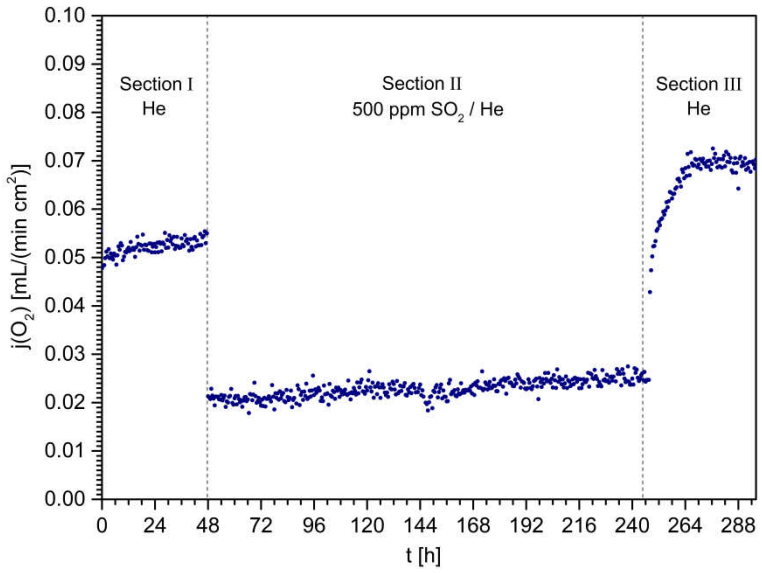

Figure 17 Oxygen flux of the non-activated 85CGO-FCO membrane with alternating sweep gas compositions between He in Section I, 500 ppm SO_2 / He in Section II and He in Section III.

Conclusions

The dual phase composite 85CGO-FCO is the most efficient and stable oxygen transport membrane in comparison to the higher spinel content (40 wt%) counterpart composite that was investigated in detail. The secondary phase GCFCO in combination with FCO phase apparently provides the necessary electronic conductivity while CGO contributes to the ionic transport in the membrane. The membrane has proven to be stable on exposure to chemical gas mixtures representing the flue gas condition in industrial ambiance during oxyfuel combustion process. Both short term and long term stability test have validated the stability of the phases with no traces of any chemical reactions and phase changes as observed in the post characterization of the tested samples. Under differential oxygen partial pressure gradient, high spinel content composite (60CGO-FCO) show spinel enrichment on the high p_{O2} side leading to phase segregation over a period of time. Nevertheless, 85CGO-FCO shows minimal phase segregation due to lower spinel content in addition to superior oxygen flux marking the composition as the optimum for application within the investigated range. Additionally the oxygen flux of an 85CGO-FCO membrane was measured with 500 ppm SO_2 in the sweep gas. Two overlapping effects occurred. The first effect entailed a gradual improvement of the oxygen flux over the course of the 300 h long term experiment that is attributed to phase segregation of the spinel and the associated slow surface roughening. The second effect entailed an instantaneous oxygen flux drop by nearly two thirds after mixing 500 ppm of SO_2 to the sweep gas due to the rapid adsorption of SO_2, followed by a slow recovery of the oxygen flux after switching the sweep gas back to pure helium caused by the slow desorption kinetics of SO_2 over the course of 24 h. Nevertheless, the permeation rate remained stable revealing the stability of the membrane material in presence of SO_2.

Acknowledgements

This work has been funded by the Federal Ministry of Education and Research, Germany (BMBF) (Grant: 03EK3032) and the European Commission via the FP7 project GREEN-CC (Grant agreement no. 608524). The authors acknowledge the support of Dr. D. Sebold for part of the SEM analyses, Dr. J. Sohn for Rietveld refinement of X-ray analysis data, Mr. S. Heinz for his technical assistance in sample preparation (Forschungszentrum Jülich GmbH) and Mr. L. E. Powell (ORNL) for helping with the short term stability test setup.

References

[1] J. Sunarso, S. Baumann, J.M. Serra, W.A. Meulenberg, S. Liu, Y.S. Lin, J.C. Diniz da Costa, Mixed ionic–electronic conducting (MIEC) ceramic-based membranes for oxygen separation, Journal of Membrane Science, 320 (2008) 13-41.
[2] C. Karakaya, R.J. Kee, Progress in the direct catalytic conversion of methane to fuels and chemicals, Progress in Energy and Combustion Science, 55 (2016) 60-97.
[3] B.A. van Hassel, Oxygen transfer across composite oxygen transport membranes, Solid State Ionics, 174 (2004) 253-260.
[4] M. Czyperek, P. Zapp, H.J.M. Bouwmeester, M. Modigell, K.V. Peinemann, I. Voigt, W.A. Meulenberg, L. Singheiser, D. Stöver, MEM-BRAIN gas separation membranes for zero-emission fossil power plants, Energy Procedia, 1 (2009) 303-310.
[5] J.M. Serra, J. Garcia-Fayos, S. Baumann, F. Schulze-Küppers, W.A. Meulenberg, Oxygen permeation through tape-cast asymmetric all-La0.6Sr0.4Co0.2Fe0.8O3-δ membranes, Journal of Membrane Science, 447 (2013) 297-305.
[6] S. Baumann, J.M. Serra, M.P. Lobera, S. Escolástico, F. Schulze-Küppers, W.A. Meulenberg, Ultrahigh oxygen permeation flux through supported

Ba0.5Sr0.5Co0.8Fe0.2O3−δ membranes, Journal of Membrane Science, 377 (2011) 198-205.
[7] U. Nigge, H.D. Wiemhöfer, E.W.J. Römer, H.J.M. Bouwmeester, T.R. Schulte, Composites of Ce0.8Gd0.2O1.9 and Gd0.7Ca0.3CoO3−δ as oxygen permeable membranes for exhaust gas sensors, Solid State Ionics, 146 (2002) 163-174.
[8] J. Sanchez, T.T. Tsotsis, Chapter 11 Current developments and future research in catalytic membrane reactors, in: A.J. Burggraaf, L. Cot (Eds.) Membrane Science and Technology, Elsevier, 1996, pp. 529-568.
[9] V.V. Kharton, A.V. Kovalevsky, A.P. Viskup, F.M. Figueiredo, A.A. Yaremchenko, E.N. Naumovich, F.M.B. Marques, Oxygen permeability and Faradaic efficiency of Ce0.8Gd0.2O2–δ–La0.7Sr0.3MnO3–δ composites, Journal of the European Ceramic Society, 21 (2001) 1763-1767.
[10] H. Takamura, K. Okumura, Y. Koshino, A. Kamegawa, M. Okada, Oxygen Permeation Properties of Ceria-Ferrite-Based Composites, Journal of Electroceramics, 13 (2004) 613-618.
[11] M.P. Lobera, J.M. Serra, S.P. Foghmoes, M. Søgaard, A. Kaiser, On the use of supported ceria membranes for oxyfuel process/syngas production, Journal of Membrane Science, 385-386 (2011) 154-161.
[12] Z. Cao, H. Jiang, H. Luo, S. Baumann, W.A. Meulenberg, J. Assmann, L. Mleczko, Y. Liu, J. Caro, Natural gas to fuels and chemicals: Improved methane aromatization in an oxygen-permeable membrane reactor, Angewandte Chemie - International Edition, 52 (2013) 13794-13797.
[13] H. Luo, T. Klande, Z. Cao, F. Liang, H. Wang, J. Caro, A CO2-stable reduction-tolerant Nd-containing dual phase membrane for oxyfuel CO2 capture, Journal of Materials Chemistry A, 2 (2014) 7780-7787.
[14] J. Zhou, X. Tang, D. He, C. Wu, Y. Zhang, W. Ding, Y. Jin, C. Sun, Oxygen permeability and CO2-tolerance of Ce0.9Gd0.1O2−δ – SrCo0.8Fe0.1Nb0.1O3−δ dual-phase membrane, Journal of Alloys and Compounds, 646 (2015) 204-210.
[15] S. Engels, T. Markus, M. Modigell, L. Singheiser, Oxygen permeation and stability investigations on MIEC membrane materials under operating conditions for power plant processes, Journal of Membrane Science, 370 (2011) 58-69.
[16] M. Ramasamy, S. Baumann, J. Palisaitis, F. Schulze-Küppers, M. Balaguer, D. Kim, W.A. Meulenberg, J. Mayer, R. Bhave, O. Guillon, M. Bram, Influence of Microstructure and Surface Activation of Dual-Phase Membrane Ce0.8Gd0.2O2-δ-FeCo2O4 on Oxygen Permeation, Journal of the American Ceramic Society, 99 (2016) 349-355.
[17] M. Ramasamy, S. Baumann, A. Opitz, R. Iskandar, J. Mayer, D. Udomsilp, U. Breuer, M. Bram, Phase Interaction And Distribution In Mixed Ionic Electronic Conducting Ceria-Spinel Composites, Ceramic Engineering and Science Proceedings, 37 (2016) (In press).
[18] X. Zhu, H. Wang, W. Yang, Relationship between homogeneity and oxygen permeability of composite membranes, Journal of Membrane Science, 309 (2008) 120-127.
[19] N. Bahlawane, P.H.T. Ngamou, V. Vannier, T. Kottke, J. Heberle, K. Kohse-Hoinghaus, Tailoring the properties and the reactivity of the spinel cobalt oxide, Physical Chemistry Chemical Physics, 11 (2009) 9224-9232.
[20] M. Sun, X. Chen, L. Hong, Influence of the interfacial phase on the structural integrity and oxygen permeability of a dual-phase membrane, ACS Applied Materials and Interfaces, 5 (2013) 9067-9074.
[21] U. Pippardt, J. Boer, C. Bollert, A. Hoffmann, M. Heidenreich, R. Kriegel, M. Schulz, A. Simon, Performance and Stability of Mixed Conducting Composite Membranes Based on Substituted Ceria, J. Ceram. Sci. Technol., 5 (2014) 309-316.
[22] Y. Lin, S. Fang, D. Su, K.S. Brinkman, F. Chen, Enhancing grain boundary ionic conductivity in mixed ionic-electronic conductors, Nat Commun, 6 (2015) 6824.
[23] S. Baumann, P. Niehoff, F. Schulze-Küppers, M. Ramasamy, W.A. Meulenberg, O. Guillon, The role of solid-gas electrochemical interfaces for mixed ionic electronic conducting oxygen transport membranes, in: ECS Transactions, 2015, pp. 21-33.
[24] I.V. Belova, M.J. Brown, G.E. Murch, Analysis of kinetic demixing in a mixed oxide (A,B)O in an oxygen potential gradient, Acta Materialia, 51 (2003) 1821-1826.

Published in: *Journal of Membrane Science 544 (2017) 278–286*

[25] M. Martin, Materials in thermodynamic potential gradients, The Journal of Chemical Thermodynamics, 35 (2003) 1291-1308.
[26] H.I.Y. J. O. Hong, Electric Field-Induced Unmixing in Mixed Ferrite Spinel (Co,Fe)3O4, Advances in Science and Technology, 46 (2006) 11-20.
[27] D. Schlehuber, E. Wessel, L. Singheiser, T. Markus, Long-term operation of a La0.58Sr0.4Co0.2Fe0.8O3-δ-membrane for oxygen separation, Journal of Membrane Science, 351 (2010) 16-20.